IJMMM International Journal of Minerals, Metallurgy and Materials 矿物冶金与材料学报（英文版）

Kinetically controlled synthesis of atomically precise Ag nanoclusters for the catalytic reduction of 4-nitrophenol

Xian-hu Liu, Fei-hong Wang, Cong-ying Shao, Gang-feng Du, and Bing-qing Yao

Cite this article as:
Xian-hu Liu, Fei-hong Wang, Cong-ying Shao, Gang-feng Du, and Bing-qing Yao, Kinetically controlled synthesis of atomically precise Ag nanoclusters for the catalytic reduction of 4-nitrophenol, *Int. J. Miner. Metall. Mater.*, 28(2021), No. 10, pp. 1716-1725. https://doi.org/10.1007/s12613-020-2186-x

View the article online at SpringerLink or IJMMM Webpage.

International Journal of Minerals, Metallurgy and Materials
Volume 28, Number 10, October 2021, Page 1716
https://doi.org/10.1007/s12613-020-2186-x

Kinetically controlled synthesis of atomically precise Ag nanoclusters for the catalytic reduction of 4-nitrophenol

Xian-hu Liu[1),*], *Fei-hong Wang*[2),*], *Cong-ying Shao*[1)], *Gang-feng Du*[3)], *and Bing-qing Yao*[4)]

1) Department of Chemistry, Huaibei Normal University, Huaibei 235000, China
2) Henan Key Laboratory of High-temperature Structural and Functional Materials, National Joint Engineering Research Center for Abrasion Control and Molding of Metal Materials, Henan University of Science and Technology, Luoyang 471003, China
3) Department of Public Teaching, Nanyang Medical College, Nanyang 473061, China
4) School of Materials Science and Engineering, Nanyang Technological University, Singapore 639798, Singapore
(Received: 3 August 2020; revised: 3 September 2020; accepted: 4 September 2020)

Abstract: Synthesizing atomically precise Ag nanoclusters (NCs), which is essential for the general development of NCs, is quite challenging. In this study, we report the synthesis of high-purity atomically precise Ag NCs via a kinetically controlled strategy. The Ag NCs were prepared using a mild reducing agent via a one-pot method. The as-prepared Ag NCs were confirmed to be Ag_{49}(D-pen)$_{24}$ (D-pen: D-penicillamine) on the basis of their matrix-assisted laser desorption ionization time-of-flight mass spectrometric and thermogravimetric characteristics. The interfacial structures of the Ag NCs were illustrated by proton nuclear magnetic resonance and Fourier-transform infrared spectroscopy. The Ag NCs were supported on activated carbon (AC) to form Ag NCs/AC, which displayed excellent activity for the catalytic reduction of 4-nitrophenol with a kinetic reaction rate constant k of 0.21 min^{-1}. Such a high k value indicates that the composite could outperform several previously reported catalysts. Moreover, the catalytic activity of Ag NCs/AC remained nearly constant after six times of recycle, which suggests its excellent stability.

Keywords: Ag nanoclusters; D-penicillamine; sodium cyanoborohydride; catalysis; 4-nitrophenol

1. Introduction

Over the last few decades, advances in nanoscience have promoted explosive progress in several areas of research [1−8]. Among the numerous nanoscale materials obtained thus far, metal nanoclusters (NCs) consisting of several to hundreds of atoms have attracted broad attention [9−18]. Compared with atoms, molecules, and nanocrystals, metal NCs present two unique characteristics. First, the sizes of NCs fall between those of nanocrystals and atoms/molecules and are comparable with the Fermi wavelength of electrons; thus, NCs display discrete electronic states and size-dependent band gaps. Second, NCs are usually denoted $M_n(SR)_m$, where n and m are the numbers of metal atoms and ligands, respectively, and have particular metal–kernel and metal–ligand interfacial structures. Hence, NCs are essentially inorganic–organic hybrid compounds possessing distinct absorption and inter-particle packing properties. These characteristics endow NCs with distinct physical and chemical properties, such as abundant surface and interfacial sites [19], enhanced photoluminescence [20−21], magnetism [22], and nonlinear optical properties. Consequently, metal NCs have found enormous potential applications in the areas of energy conversion [15], catalysis [19], biomedicine [23], bioimaging [20,24], and sensors.

Among the various NCs currently available, gold NCs are the most extensively studied owing to their high stability. Several well-defined gold NCs, such as Au_{22} [25], Au_{25} [26], Au_{36} [27], Au_{38} [28], and Au_{144} [29], have been reported. However, fewer examples of Ag NCs have been synthesized compared with Au NCs. Thus, more efforts should be taken to prepare Ag NCs. Several physical and chemical means have been exploited to produce the NCs, and these methods can be divided into two categories, namely, thermodynamic and kinetics methods. Some NCs of a certain size and stability have been obtained via the thermodynamic method. Jin *et al.* [30], for example, devised a size-focusing methodology to synthesize atomically precise metal NCs based on

*These authors contributed equally to this work.
Corresponding author: Xian-hu Liu E-mail: liuxhv@126.com

different-sized nanoparticles with vastly different stabilities. Most NCs, such as Au_{25}, Au_{38}, and Au_{144}, are prepared through this method. Sonochemical and microwave-assisted green approaches have also been employed to prepare highly fluorescent, stable, and water-soluble Ag NCs in the presence of polymethylacrylic acid and polymethylacrylic acid + sodium salt respectively [31−32]. Pradeep's group [33−34] reported high-temperature and sunlight-mediated means to synthesize glutathione-protected atomically precise Ag NCs with luminescent and antibacterial properties. Unlike the thermodynamic method, kinetically controlled synthesis could yield NCs with well-defined sizes depending on the deliberate regulation of the kinetics of the reduction process. $Ag_9(H_2MSA)_7$ has been successfully prepared via a solid-state route in which the rate of reaction was decreased in contrast with that in solution reduction [35]. Adjusting the reaction temperature and stirring rate, regulating the pH of the solution, and selecting weak reducing agents are feasible methods to control the kinetics of the reduction process [26,36−37].

In this work, we demonstrate a kinetically controlled strategy to synthesize Ag NCs in high purity via a one-pot method. The reaction system employs a mild reducing agent, $NaBH_3CN$, to create a gentle environment. The resulting Ag NCs were supported on activated carbon (AC) to form Ag NCs/AC, which displayed excellent activity and stability for the catalytic reduction of 4-nitrophenol (4-NP).

2. Experimental

2.1. Chemicals

$AgNO_3$ (>99.999%), D-penicillamine (99%), $NaBH_3CN$ (99%), $NaBH_4$ (99%), α-cyano-4-hydroxycinnamic acid (CHCA, 98%,), and 4-NP (99%) were obtained from J&K Scientific Ltd., China. Methanol and ethanol were purchased from Sinopharm Chemical Reagent Co., Ltd., China (AR). Ultrapure water (18.2 MΩ) was used in all experiments.

2.2. Synthesis

The synthesis of Ag NCs was conducted under an air atmosphere. In a typical reaction, $AgNO_3$ (0.021 g, 0.125 mmol) was dissolved in ultrapure water (5 mL), and the resulting solution was cooled to 5°C, D-penicillamine (0.075 g, 0.5 mmol) was taken up in 5 mL of ultrapure water and then transferred to the cooled $AgNO_3$ solution via syringe. The resulting mixture was stirred at 5°C. After 20 min, 3 mL of an ice-cold aqueous solution of $NaBH_3CN$ (0.079 g, 1.25 mmol) was quickly added to the above mixture under vigorous stirring. The reaction was aged for 4 h at 5°C and 5 h at room temperature to ensure complete reaction. The product was isolated by centrifugation, and the precipitate was discarded. Excess methanol was added to the supernatant, and the mixture was allowed to stand at 4°C for 3 h. The precipitated solid was purified repeatedly by centrifugation. Finally, the Ag NCs were dried overnight in a vacuum at room temperature.

In a typical experiment, 10 mg of AC (XC-72) was dispersed in 15 mL of ultrapure water under ultrasonication for 20 min. Then, 0.2 mL of Ag NCs dissolved in ultrapure water (1 mg/mL) was added to the above AC suspension. The catalysts were separated by centrifugation at 10000 r/min after stirring for 12 h. A clear supernatant solution indicated the nearly complete absorption of NCs on the support. The catalysts were washed thrice with ultrapure water and ethanol in turn. Finally, the catalysts were dried for 5 h in a vacuum at room temperature and dispersed in water for further use.

2.3. Characterization

Ultraviolet visible (UV–Vis) absorption data were collected by a UV-3600 UV–Vis-NIR spectrophotometer (Shimadzu, Japan). Transmission electron microscopy (FEI Technai-F30, USA) with an accelerating voltage of 200 kV was employed to observe the size and morphology of the Ag NCs. The size distributions of the Ag NCs were analyzed using Nano Measurer software. Proton nuclear magnetic resonance (^{1}H-NMR) experiments were conducted using a 500 MHz Advance NMR spectrometer (Bruker, Germany). The Ag NCs and D-penicillamine were dissolved in deuterium oxide, and TMS was used as an internal standard. Matrix-assisted laser desorption ionization time-of-flight mass spectrometry (MALDI-TOF MS) was conducted on an Autoflex Max MALDI-TOF mass spectrometer (Bruker, Germany). X-ray photoelectron spectroscopy (XPS) measurements were performed using a VG Thermo ESCALAB 250 spectrometer (VG Scientific, USA) operated at 200 W. Binding energies were calibrated against the C 1s line. Fourier-transform infrared spectroscopy (FTIR) was conducted using a NICOLET iS50 FT-IR (Thermo Scientific, USA). Thermogravimetry (TG) experiments were performed on a TG209F1 instrument (Netzsch, Germany).

2.4. Catalytic experiments

A mixture of 4-NP (7 mg, 0.03 mmol) and Ag NCs/AC (10 mg) was dissolved in 15 mL of ultrapure water. Then, excess $NaBH_4$ (38 mg, 1.0 mmol) was added to the above suspension, and the mixture was stirred at room temperature. UV–Vis absorption was used to monitor the progress of the reaction at different time intervals. The catalysts were centrifuged and washed thrice with ultrapure water for the next cycle after completion of the catalytic reaction.

3. Results and discussion

The kinetics of a reduction process plays a great role in the preparation of NCs. Changes in the reducing agent and temperature and introduction of additives are feasible means to control the kinetics of a reduction process. In our previous

work, $NaBH_4$, a strong reducing agent, was used to prepare penicillamine-protected Ag_{20} NCs [38]. In the present work, $NaBH_3CN$, a weak reducing agent, was used to control the reduction kinetics. UV–Vis absorption was employed to track the process of NC formation (Fig. 1(a)). At the initial stage of the preparation process, a distinct peak at 518 nm corresponding to Ag_{20} NCs was observed; this peak decomposed rapidly within 2 h. The peak at 425 nm (Fig. 1(a)) corresponding to Ag nanoparticles revealed weakening and redshifting during the reaction process, thereby indicating that the Ag nanoparticles were transformed into smaller-sized NCs. Peaks at 600 and 660 nm emerged and gradually intensified, thus suggesting that new NCs with contents increasing with the reaction time are formed.

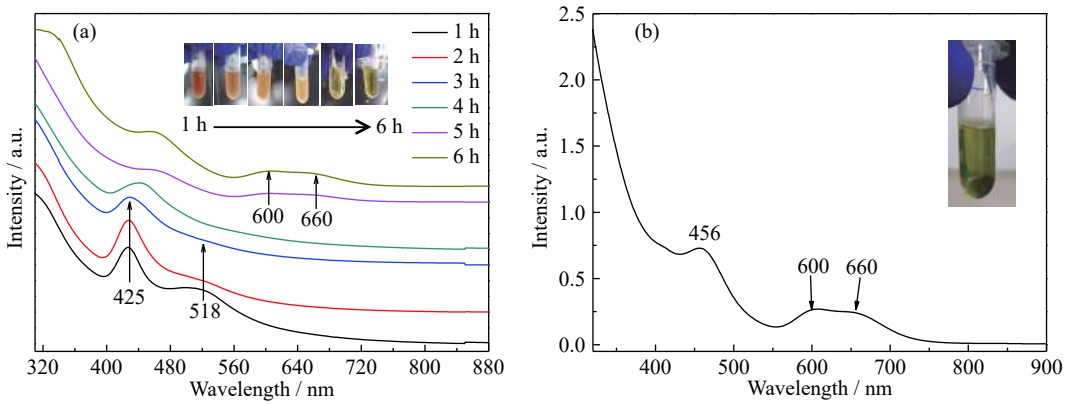

Fig. 1. (a) UV–Vis absorption spectra of products at different reaction times. The inset shows photographs of the products. (b) UV–Vis absorption spectrum of the as-synthesized Ag NCs. The inset shows a photograph of the as-synthesized Ag NC aqueous solution.

The solution color may also reflect the progress of the formation of NCs. During the preparation of Ag_{20} NCs, the solution turned from colorless to black within several minutes after the addition of $NaBH_4$, which indicates that some large-sized Ag nanoparticles were formed at the initial stage and that the reduction process proceeded rapidly. In the present work, the solution first changed to brownish red (inset, Fig. 1(a)) when the reducing agent was introduced, thus suggesting that small-sized NCs were produced at this stage. In general, the size distribution of the precursor remarkably influences the size of the final NCs. Thus, the NCs formed under mild reducing condition in this work should be different from the Ag_{20} NCs. In the present work, the color of the Ag NCs was dark green (inset in Fig. 1(b)) while that of the Ag_{20} NCs was deep red [38]. The different size distributions of the precursors may further be reflected by the reaction time. During the preparation of Ag_{20} NCs, the large mass of Ag nanoparticles formed at the initial stages of the reaction required a long time for etching. By contrast, the small-sized NCs and few Ag nanoparticles produced in the present work were easily transformed into the final NCs. Therefore, 48 h was needed to produce Ag_{20} NCs [38], but only 9 h was necessary to complete the reaction in the present work.

The as-synthesized Ag NCs displayed optical properties different from those Ag NCs reported earlier, such as $Ag_7(H_2MSA)_7$ [39], $Ag_8(H_2MSA)_8$ [39], $Ag_9(H_2MSA)_7$ [35], $Ag_{11}(SG)_7$ [40], $Ag_{14}(SG)_{11}$ [41], $Ag_{32}(SG)_{19}$ [42], and $Ag_{44}(SR)_{30}$ [43]. Three distinct peaks at approximately 456, 600, and 660 nm were observed in the UV–Vis absorption spectrum of the as-synthesized Ag NCs (Fig. 1(b)), which indicates that the product is of high purity; a mixture of several NCs with different sizes usually yields a featureless absorption spectrum. The presence of Ag nanoparticles could be excluded because no surface plasmon resonance absorption was observed in the absorption spectrum obtained. According to previous reports [39], the absorption peaks at 600 and 660 nm are induced by intra-band sp → sp transitions while the absorption peak at 456 nm is due to inter-band ligand/d-band → sp-band transitions.

MALDI-TOF MS was used for ionization and molecular weight measurements with CHCA as the matrix to confirm the molecular composition of the as-synthesized Ag NCs. Two peaks at approximately *m*/*z* 6796 (*m* is the mass and *z* is the electrical charge) and 8844 were detected in negative mode (Fig. 2(a)). However, the precise composition of the as-synthesized Ag NCs could not be confirmed on account of the low resolution of the signals. Thus, TG was employed to confirm the molecular composition of the NCs (Fig. 2(b)). The peaks at *m*/*z* 6796 and 8844 were assigned to Ag_{41}(D-pen)$_{16}$ (D-pen: D-penicillamine) and Ag_{49}(D-pen)$_{24}$, respectively. Ag_{41}(D-pen)$_{16}$ may be a fragment of Ag_{49}(D-pen)$_{24}$ because the absorption spectra obtained indicate that the as-synthesized Ag NCs is of high purity.

NMR spectroscopy is a useful method to probe the chemical environments and staple motif structures of metal–ligand interfaces. ^{1}H-NMR of both the Ag NCs and D-penicil-

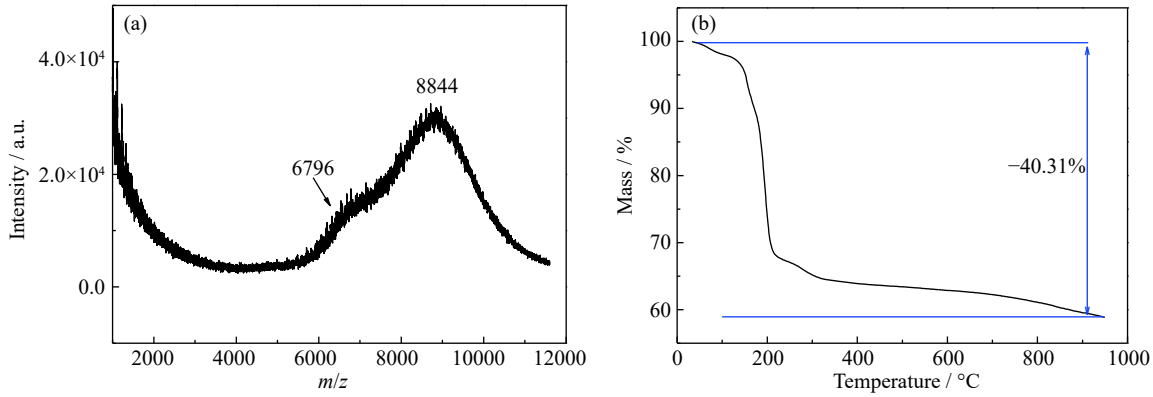

Fig. 2. (a) MALDI-TOF MS spectrum of the as-synthesized Ag NCs in negative mode. (b) Mass change of the Ag NCs vs. temperature in a nitrogen atmosphere.

lamine was conducted (Fig. 3(a)). The spectrum of Ag NCs showed two broad peaks while that of D-penicillamine revealed three intense peaks. The merging of the two intense peaks corresponding to $–CH_3$ groups could be attributed to rapid location changes of the two $–CH_3$ groups on the surface of the NCs. The relevant peaks of the NCs broadened in comparison with those of D-penicillamine, and this phenomenon may be induced by minor differences in the staple motif structure of Ag NCs. In addition, all peaks in the spectrum of Ag NCs appeared downfield relative to those of D-penicillamine, which indicates that protons in the staple motif are affected by the –SH group, which is considered to transfer electrons to the Ag core when the S–Ag bond is formed. The FTIR spectra of Ag NCs and D-penicillamine are given in Fig. 3(b). The spectrum of D-penicillamine displayed various characteristic peaks corresponding to the different stretching and bending modes of the bonds. For example, the peaks at 1464 and 1380 cm^{-1} could be attributed to the scissoring vibrations of methyl ($–CH_3$) groups, while the peaks at 1096 and 1052 cm^{-1} could be assigned to the stretching vibrations of C–N and C–O, respectively. Several of these vibrational modes were also observed in the spectrum of Ag NCs. However, the peaks of the scissoring vibrations of $–CH_3$ groups in the Ag NCs red-shifted when the staple motifs were formed, suggesting that the $–CH_3$ groups of the ligand were located close to the core of the NCs. Some broadening (e.g., 1456 and 1346 cm^{-1}) and merging (e.g., 1626 and 1118 cm^{-1}) of peaks caused by metal–ligand interactions and electron transfer were also observed. Most importantly, the absence of S–H stretching at 2507 cm^{-1} in the spectrum of the Ag NCs indicated the binding of −SH to the Ag core, which is consistent with previously reported results for Ag NC formation.

XPS was utilized to study the chemical composition and valence states of the Ag NCs (Fig. 4). The XPS survey spectrum obtained suggested the presence of C, S, O, N, and Ag elements. The peak of S $2p_{3/2}$ appearing at 161.8 eV was assigned to S in the form of thiolate because this peak is located close to the reported value of metal sulfides. Ag may be expected in the forms of Ag^+ and Ag^0 because the binding energy of Ag $3d_{5/2}$ (368.2 eV) is between those of Ag^+ and bulk Ag^0.

4-Aminophenol (4-AP) is a useful and important chemical with extensive applications as an inhibitor, painkiller, feb-

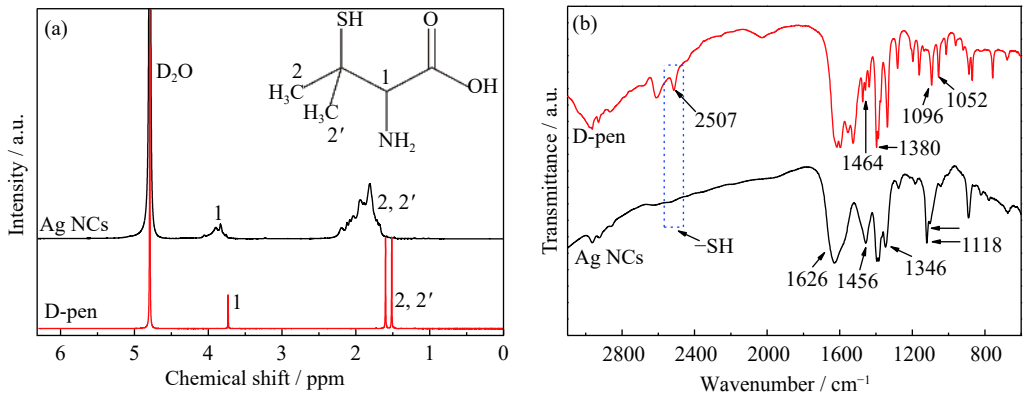

Fig. 3. (a) ^{1}H-NMR spectra of the Ag NCs and D-penicillamine (D-pen) in D_2O solution. The inset displays the chemical structure of D-penicillamine. Number 1 represents –CH group and number 2 (2') denotes $–CH_3$ group. (b) FTIR spectra of the Ag NCs and D-penicillamine. The dotted rectangle shows the position of the S–H vibrational frequency peak.

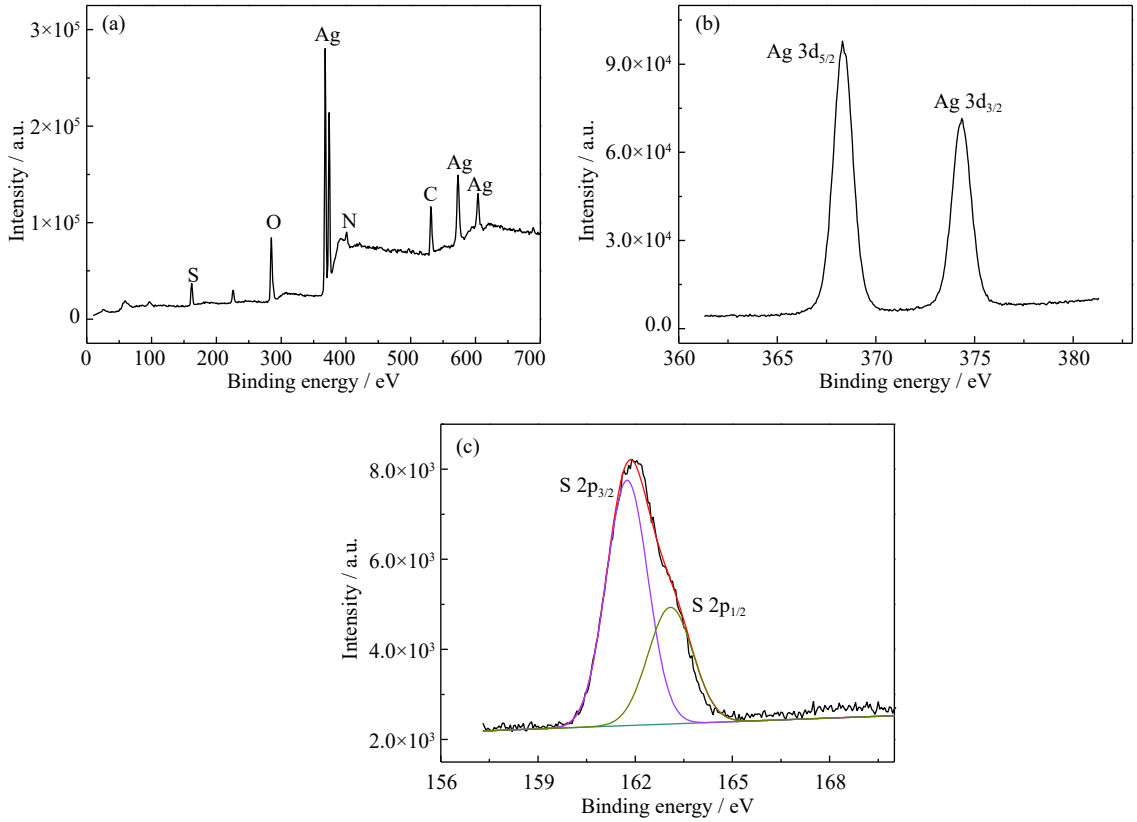

Fig. 4. XPS (a) survey, (b) Ag 3d, and (c) S 2p spectra of the Ag NCs.

rifuge, anticorrosion lubricant, and eikonogen [44–46]. Noble metal nanoparticles have been intensively investigated as catalysts for the efficient production of 4-AP using 4-NP as the reactant and $NaBH_4$ as the reducing agent. Therefore, the conversion of 4-NP to 4-AP in the presence of an excess amount of $NaBH_4$ was exploited in this work as a model reaction to evaluate the catalytic activities of the as-synthesized Ag NCs quantitatively. A yellow solution was immediately formed when $NaBH_4$ was added to the 4-NP solution. According to previous reports [47], the generation of 4-nitrophenolate ions under alkaline condition may be manifested by a strong absorption peak at 400 nm. The Ag NCs displayed catalytic activity for the reduction of 4-NP (Fig. 5(a)). However, aggregation of Ag NCs was observed during the reduction process. As seen in the inset in Fig. 5(a), the color of the Ag NC aqueous solution changed from dark green to dark brown after the introduction of $NaBH_4$ and a precipitate was obtained after centrifugation. This finding reveals the instability of Ag NCs under the reduction conditions employed. Subsequently, the Ag NCs were absorbed on the surface of AC to form Ag NCs/AC composites and enhance the stability of the catalyst. The TEM, high-angle annular dark field, and elemental mapping images show that the Ag NCs are dispersed uniformly on the AC (Figs. 6(a)–6(d) and 6(g)–6(l)). The sizes of the AC spheres and Ag NCs were approximately 50 and 2 nm respectively. In the control experiment, the intensity of the absorption peak at 400 nm was nearly invariant in the absence of Ag NCs when AC was added to the solution of 4-nitrophenolate ions (Fig. 5(b)). This result indicates that AC exhibits no catalytic activity for the reduction of 4-NP. However, the absorption intensity of 4-nitrophenolate ions at 400 nm decreased quickly with time after the introduction of Ag NCs/AC (Fig. 5(c)). Two new peaks also appeared at 230 and 300 nm, thus suggesting the successful conversion of 4-NP to 4-AP. The peak at 400 nm nearly completely disappeared after 18 min, and the color of the solution changed from yellow to colorless. Therefore, Ag NCs/AC show excellent catalytic activity for the reduction of 4-NP to 4-AP.

According to previous reports [48], the concentration of borohydride anion remains nearly constant during the reaction process owing to the large excess of $NaBH_4$ compared with 4-NP. Thus, the catalytic process could be regarded as a pseudo-first order reaction according to the kinetic equation of $\ln(C_t/C_0) = -kt$. Herein, C_0 is the initial concentration of 4-NP before the reduction and C_t is the instantaneous concentration of 4-NP throughout the reaction. C_t/C_0 was calculated from the relative intensity of absorbance (A_t/A_0) at 400 nm, and $\ln(C_t/C_0)$ versus time could be estimated on the basis of changes in absorbance with respect to time. As shown in Fig. 5(d), a good linear relationship between $\ln(C_t/C_0)$ and t was observed, thereby indicating that the reduction reaction

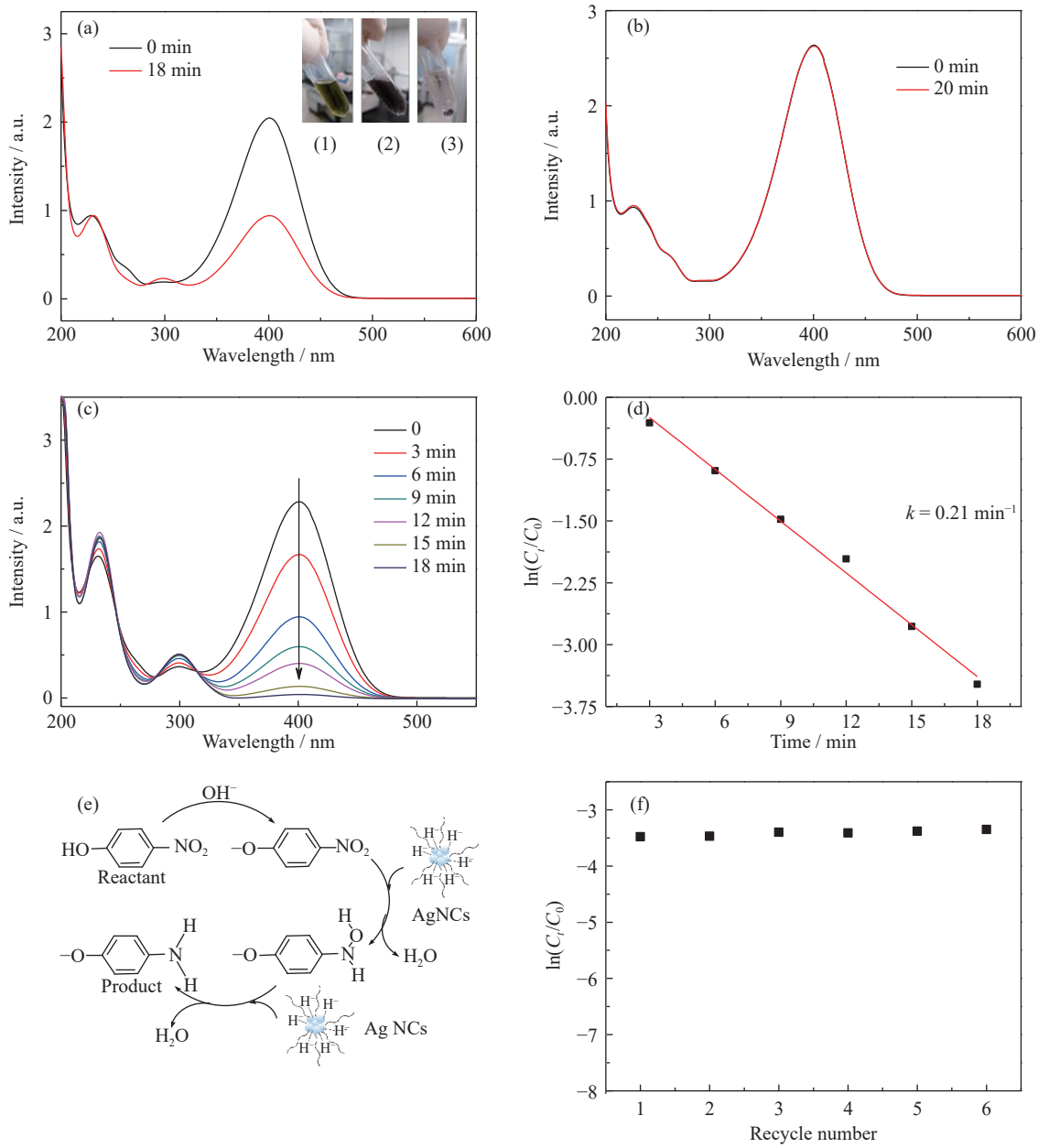

Fig. 5. UV–Vis absorption spectra of the reduction of 4-nitrophenol (4-NP) by (a) Ag NCs, (b) AC, and (c) Ag NCs/AC. The insets in (a) show photographs of the Ag NCs aqueous solution (1) before and (2) after addition of $NaBH_4$ and (3) the solution in inset (2) after centrifugation. (d) Plot of the logarithm of C_t/C_0 vs. reduction time, where C_t is the concentration of 4-NP during the reduction process, and C_0 is the initial concentration of 4-NP before reduction. (e) Proposed mechanism of the hydrogenation of 4-NP catalyzed by Ag NCs/AC. (f) Recyclability of Ag NCs/AC for the reduction of 4-NP.

follows pseudo-first-order kinetics. The kinetic reaction rate constant k of the Ag NCs/AC was obtained from the slope of the linear relationship and found to be 0.21 min^{-1}. This k value is larger than those of several previously reported catalysts (Table 1) and may be explained in view of four aspects. First, the ultra-small sizes of Ag NCs with high percentage of surface atoms are the main active sites of the catalyst and display excellent catalytic activity. Second, the molecular properties of Ag NCs possessing a homogeneous surface chemical environment favor absorption of the substrate molecules. Third, the D-penicillamine ligand possesses the properties of water solubility and small size. Ag NCs protected by D-penicillamine have good affinity to 4-NP molecules and low coverage of active sites. Finally, the uniform and stable dispersion of Ag NCs on the AC improves the availability and recyclability of the catalyst. A possible mechanism based on the above results is proposed for the hydrogenation of 4-NP, as shown in Fig. 5(e). First, $NaBH_4$ is decomposed by hydrolysis, and active hydrogen is formed. This hydrogen is then adsorbed on the active sites of Ag NCs. 4-nitrophenolate ions

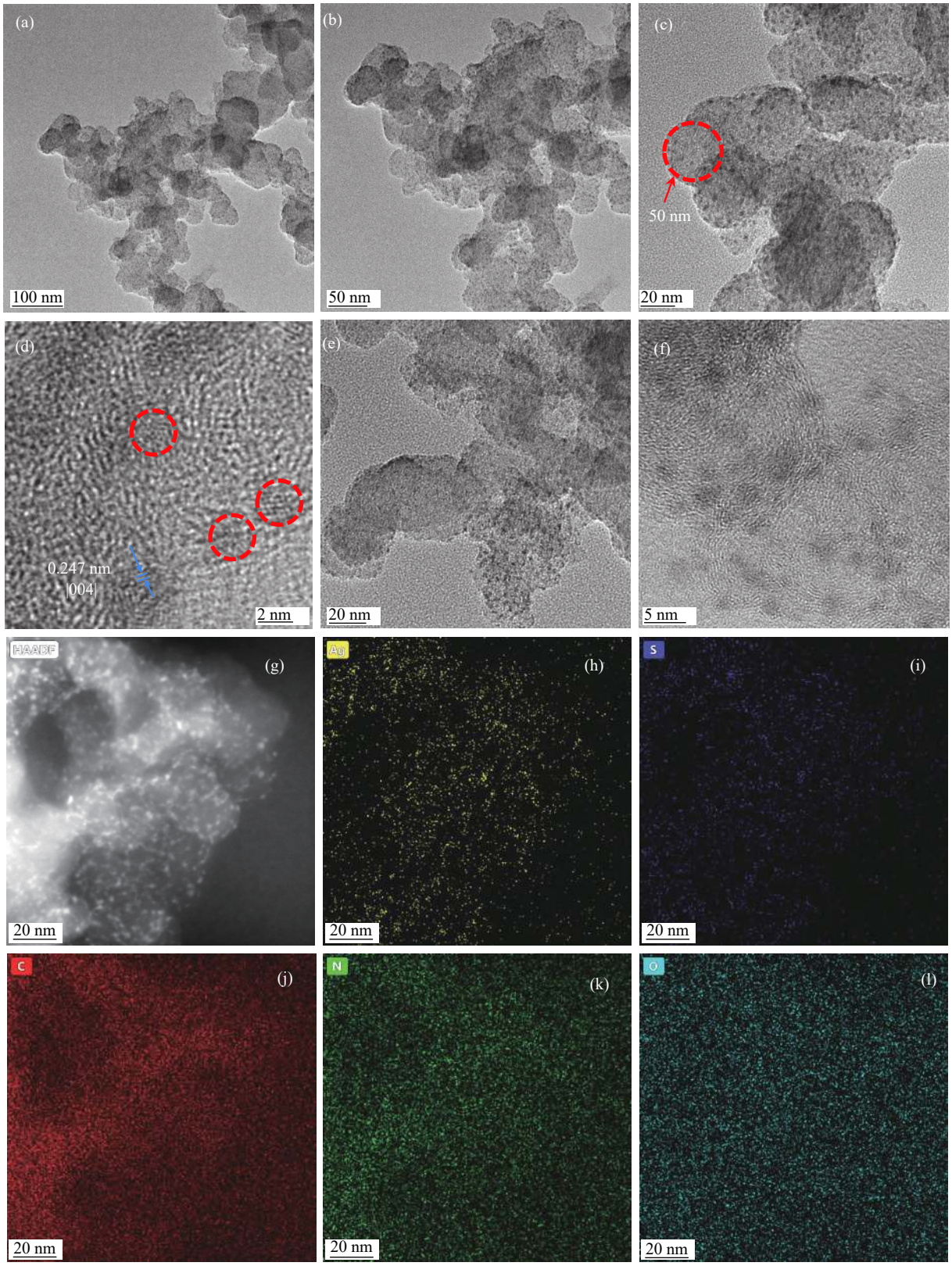

Fig. 6. (a, b, c, d) TEM micrographs of the Ag NCs/AC recorded at different magnifications. (e, f) TEM micrographs of Ag NCs/AC after six cycles of catalytic reaction. (g) High-angle annular dark field images of the Ag NCs/AC. Elemental mappings of (h) Ag, (i) S, (j) C, (k) N, and (l) O in Ag NCs/AC.

react with active hydrogen to give 4-hydroxylaminophenolate ions, which could further react with hydrogen to generate 4-AP. The activity of the catalyst remained nearly unchanged after six recycles (Fig. 5(f)). TEM images of the Ag NCs/AC after six recycles were obtained, and the sizes of the reused Ag NCs were comparable with that of the as-synthesized Ag NCs (Figs. 6(e) and 6(f)). These results reflect the excellent stability of the catalyst.

Table 1. Comparison of various reported catalysts for 4-nitrophenol reduction

Catalyst	Rate constants / min^{-1}	Initial concentration of 4-NP / mM	Amount of catalysts / ($mg \cdot mL^{-1}$)	Temperature / °C	Ref.
Pt–Au ANCs	0.080	0.01	0.04	25	[49]
$Ni_{96}Pt_4$ nanoparticles	0.116	0.085	0.00174	30	[50]
Cat_3Au_1	0.01476	3	~0.333	25	[51]
p(AAm)-CB-Ag	0.037	15	0.01924	30	[52]
Spongy Au	0.126	0.103	2	25	[53]
Au@Ag nanorods	0.0274	0.18	—	—	[54]
Dendritic Pt	~0.045	0.1	—	—	[48]
AC/Ag NCs	0.21	3.5	0.013	25	This work

4. Conclusion

A one-pot and kinetically controlled strategy was employed to synthesize water-soluble and atomically precise Ag NCs. The Ag NCs were characterized to be Ag_{49}(D-pen)$_{24}$ by MALDI-TOF MS and TG analyses. The CH_3 groups of the ligand were located close to the core of the NCs when the staple motifs were formed. The Ag NCs were supported on AC to form Ag NCs/AC, which showed excellent activity and stability for the catalytic reduction of 4-NP to 4-AP with a kinetic rate constant k of 0.21 min^{-1}. This k value is even higher than those of some previously reported catalysts. The atomically precise Ag NCs developed in the present work provide a well-defined model for the investigation and application of Ag NCs. For example, the excellent catalytic properties of Ag NCs offer a prerequisite for discussion on the catalytic mechanism.

Acknowledgements

This work was financially supported by the Huaibei Normal University Doctoral Research Start-up Funding (No. 15601012), the Natural Science Foundation of Anhui Provincial Department of Education (No. KJ2019A0598), the Excellent Young Talents Fund Program of Higher Education Institutions of Anhui Province, China (No. gxyq2019168), and the Team of Superior Discipline of Chemistry (No. GFXK202108).

References

[1] K.M. Pan, F.H. Wang, S.Z. Wei, S.H. Siyal, Y.P. Ren, L.J. Xu, X.C. Wu, and Q.K. Li, Low-temperature solution synthesis and characterization of enhanced titanium dioxide photocatalyst on tailored mesoporous γ-Al_2O_3 support, *Compos. Commun.*, 19(2020), p. 82.

[2] K.M. Pan, K.N. Shan, S.Z. Wei, Y. Zhao, L.J. Xu, J.M. Zhu, and H.H. Wu, Two-step alcohothermal synthesis and characterization of enhanced visible-light-active WO_3-coated TiO_2 heterostructure, *Ceram. Int.*, 46(2020), No. 2, p. 2102.

[3] O. Velgosova, E. Čižmárová, J. Málek, and J. Kavuličova, Effect of storage conditions on long-term stability of Ag nanoparticles formed via green synthesis, *Int. J. Miner. Metall. Mater.*, 24(2017), No. 10, p. 1177.

[4] Y.B. Wu, J. Bi, T. Lou, T.B. Song, and H.Q. Yu, Preparation of a novel PAN/cellulose acetate-Ag based activated carbon nanofiber and its adsorption performance for low-concentration SO_2, *Int. J. Miner. Metall. Mater.*, 22(2015), No. 4, p. 437.

[5] Z.M. Zheng, H.H. Wu, H.D. Liu, Q.B. Zhang, X. He, S.C. Yu, V. Petrova, J. Feng, R. Kostecki, P. Liu, D.L. Peng, M.L. Liu, and M.S. Wang, Achieving fast and durable lithium storage through amorphous FeP nanoparticles encapsulated in ultrathin 3D P-doped porous carbon nanosheets, *ACS Nano*, 14(2020), No. 8, p. 9545.

[6] K.M. Pan, K.N. Shan, S.Z. Wei, K.K. Li, J.M. Zhu, S.H. Siyal, and H.H. Wu, Enhanced photocatalytic performance of WO_{3-x} with oxygen vacancies via heterostructuring, *Compos. Commun.*, 16(2019), p. 106.

[7] H.H. Wu, Q.Q. Meng, H. Huang, C.T. Liu, and X.L. Wang, Tuning the indirect–direct band gap transition in the $MoS_{2-x}Se_x$ armchair nanotube by diameter modulation, *Phys. Chem. Chem. Phys.*, 20(2018), No. 5, p. 3608.

[8] Z.G. Wang, H.H. Wu, Q. Li, F. Besenbacher, X.C. Zeng, and M.D. Dong, Self-scrolling MoS_2 metallic wires, *Nanoscale*, 10(2018), No. 38, p. 18178.

[9] R.C. Jin, Quantum sized, thiolate-protected gold nanoclusters, *Nanoscale*, 2(2010), No. 3, p. 343.

[10] A. Mathew, and T. Pradeep, Noble metal clusters: Applications in energy, environment, and biology, *Part. Part. Syst. Charact.*, 31(2014), No. 10, p. 1017.

[11] Z.B. Gan, N. Xia, and Z.K. Wu, Discovery, mechanism, and application of antigalvanic reaction, *Acc. Chem. Res.*, 51(2018), No. 11, p. 2774.

[12] S.X. Wang, Q. Li, X. Kang, and M.Z. Zhu, Customizing the structure, composition, and properties of alloy nanoclusters by metal exchange, *Acc. Chem. Res.*, 51(2018), No. 11, p. 2784.

[13] Q.F. Yao, T.K. Chen, X. Yuan, and J.P. Xie, Toward total synthesis of thiolate-protected metal nanoclusters, *Acc. Chem. Res.*,

51(2018), No. 6, p. 1338.
[14] Z. Wang, Q.P. Qu, H.F. Su, P. Huang, R.K. Gupta, Q.Y. Liu, C.H. Tung, D. Sun, and L.S. Zheng, A novel 58-nuclei silver nanowheel encapsulating a subvalent Ag_6^{4+} kernel, *Sci. China Chem.*, 63(2020), No. 1, p. 16.
[15] Z. Wang, H.F. Su, M. Kurmoo, C.H. Tung, D. Sun, and L.S. Zheng, Trapping an octahedral Ag_6 kernel in a seven-fold symmetric Ag_{56} nanowheel, *Nat. Commun.*, 9(2018), No. 1, art. No. 2094.
[16] Z. Wang, H.F. Su, C.H. Tung, D. Sun, and L.S. Zheng, Deciphering synergetic core-shell transformation from $[Mo_6O_{22}@Ag_{44}]$ to $[Mo_8O_{28}@Ag_{50}]$, *Nat. Commun.*, 9(2018), art. No. 4407.
[17] J.W. Liu, L. Feng, H.F. Su, Z. Wang, Q.Q. Zhao, X.P. Wang, C.H. Tung, D. Sun, and L.S. Zheng, Anisotropic assembly of Ag_{52} and Ag_{76} vanoclusters, *J. Am. Chem. Soc.*, 140(2018), No. 5, p. 1600.
[18] S.S. Zhang, F. Alkan, H.F. Su, C.M. Aikens, C.H. Tung, and D. Sun, $[Ag_{48}(C{\equiv}C^tBu)_{20}(CrO_4)_7]$: An atomically precise silver nanocluster co-protected by inorganic and organic ligands, *J. Am. Chem. Soc.*, 141(2019), No. 10, p. 4460.
[19] G. Li, and R.C. Jin, Atomically precise gold nanoclusters as new model catalysts, *Acc. Chem. Res.*, 46(2013), No. 8, p. 1749.
[20] P. Khandelwal and P. Poddar, Fluorescent metal quantum clusters: An updated overview of the synthesis, properties, and biological applications, *J. Mater. Chem. B*, 5(2017), No. 46, p. 9055.
[21] H.Z. Yu, B. Rao, W. Jiang, S. Yang, and M.Z. Zhu, The photoluminescent metal nanoclusters with atomic precision, *Coord. Chem. Rev.*, 378(2019), p. 595.
[22] K.S. Krishna, P. Tarakeshwar, V. Mujica, and C.S.S.R Kumar, Chemically induced magnetism in atomically precise gold clusters, *Small*, 10(2014), No. 5, p. 907.
[23] Y. Tao, M.Q. Li, J.S. Ren, and X.G. Qu, Metal nanoclusters: Novel probes for diagnostic and therapeutic applications, *Chem. Soc. Rev.*, 44(2015), No. 23, p. 8636.
[24] T.T. Zhao, T.Y. Zhou, Q.H. Yao, C.L. Hao, and X. Chen, Metal nanoclusters: applications in environmental monitoring and cancer therapy, *J. Environ. Sci. Health Part C Environ. Carcinog. Ecotoxicol. Rev.*, 33(2015), No. 2, p. 168.
[25] Y. Yu, Z.T. Luo, D.M. Chevrier, D.T. Leong, P. Zhang, D.E. Jiang, and J.P. Xie, Identification of a highly luminescent $Au_{22}(SG)_{18}$ nanocluster, *J. Am. Chem. Soc.*, 136(2014), No. 4, p. 1246.
[26] M.Z. Zhu, E. Lanni, N. Garg, M.E. Bier, and R.C. Jin, Kinetically controlled, high-yield synthesis of Au_{25} clusters, *J. Am. Chem. Soc.*, 130(2008), No. 4, p. 1138.
[27] C.J. Zeng, C.Y. Liu, Y. Pei, and R.C. Jin, Thiol ligand-induced transformation of $Au_{38}(SC_2H_4Ph)_{24}$ to $Au_{36}(SPh\text{-}t\text{-}Bu)_{24}$, *ACS Nano*, 7(2013), No. 7, p. 6138.
[28] R.L. Donkers, D. Lee, and R.W. Murray, Synthesis and isolation of the molecule-like cluster $Au_{38}(PhCH_2CH_2S)_{24}$, *Langmuir*, 20(2004), No. 5, p. 1945.
[29] H.F. Qian, and R.C. Jin, Ambient synthesis of $Au_{144}(SR)_{60}$ nanoclusters in methanol, *Chem. Mater.*, 23(2011), No. 8, p. 2209.
[30] R.C. Jin, H.F. Qian, Z.K. Wu, Y. Zhu, M.Z. Zhu, A. Mohanty, and N. Garg, Size focusing: A methodology for synthesizing atomically precise gold nanoclusters, *J. Phys. Chem. Lett.*, 1(2010), No. 19, p. 2903.
[31] H.X. Xu and K.S. Suslick, Sonochemical synthesis of highly fluorescent Ag nanoclusters, *ACS Nano*, 4(2010), No. 6, p. 3209.
[32] S.H. Liu, F. Lu, and J.J. Zhu, Highly fluorescent Ag nanoclusters: Microwave-assisted green synthesis and Cr^{3+} sensing, *Chem. Commun.*, 47(2011), No. 9, p. 2661.
[33] I. Chakraborty, T. Udayabhaskararao, and T. Pradeep, High temperature nucleation and growth of glutathione protected ~Ag_{75} clusters, *Chem. Commun.*, 48(2012), No. 54, p. 6788.
[34] I. Chakraborty, T. Udayabhaskararao, G.K. Deepesh, and T. Pradeep, Sunlight mediated synthesis and antibacterial properties of monolayer protected silver clusters, *J. Mater. Chem. B*, 1(2013), No. 33, p. 4059.
[35] T.U.B. Rao, B. Nataraju, and T. Pradeep, Ag_9 quantum cluster through a solid-state route, *J. Am. Chem. Soc.*, 132(2010), No. 46, p. 16304.
[36] X. Yuan, B. Zhang, Z.T. Luo, Q.F. Yao, D.T. Leong, N. Yan, and J.P. Xie, Balancing the rate of cluster growth and etching for gram-scale synthesis of thiolate-protected Au_{25} nanoclusters with atomic precision, *Angew. Chem. Int. Ed.*, 53(2014), No. 18, p. 4623.
[37] Y. Yu, X. Chen, Q.F. Yao, Y. Yu, N. Yan, and J.P. Xie, Scalable and precise synthesis of thiolated $Au_{10–12}$, Au_{15}, Au_{18}, and Au_{25} nanoclusters via pH controlled CO reduction, *Chem. Mater.*, 25(2013), No. 6, p. 946.
[38] X.H. Liu, W.H. Ding, Y.S. Wu, C.H. Zeng, Z.X. Luo, and H.B. Fu, Penicillamine-protected Ag_{20} nanoclusters and fluorescence chemosensing for trace detection of copper ions, *Nanoscale*, 9(2017), No. 11, p. 3986.
[39] T. Udaya Bhaskara Rao, and T. Pradeep, Luminescent Ag_7 and Ag_8 clusters by interfacial synthesis, *Angew. Chem. Int. Ed.*, 49(2010), No. 23, p. 3925.
[40] A. Baksi, M.S. Bootharaju, X. Chen, H. Häkkinen, and T. Pradeep, $Ag_{11}(SG)_7$: A new cluster identified by mass spectrometry and optical spectroscopy, *J. Phys. Chem. C*, 118(2014), No. 37, p. 21722.
[41] J. Yang, N. Xia, X.N. Wang, X.H. Liu, A. Xu, Z.K. Wu, and Z.X. Luo, One-pot one-cluster synthesis of fluorescent and biocompatible Ag_{14} nanoclusters for cancer cell imaging, *Nanoscale*, 7(2015), No. 44, p. 18464.
[42] T. Udayabhaskararao, M.S. Bootharaju, and T. Pradeep, Thiolate-protected Ag_{32} clusters: Mass spectral studies of composition and insights into the Ag−thiolate structure from NMR, *Nanoscale*, 5(2013), No. 19, p. 9404.
[43] I. Chakraborty, W. Kurashige, K. Kanehira, L. Gell, H. Häkkinen, Y. Negishi, and T. Pradeep, $Ag_{44}(SeR)_{30}$: A hollow cage silver cluster with selenolate protection, *J. Phys. Chem. Lett.*, 4(2013), No. 19, p. 3351.
[44] J.F. Corbett, An historical review of the use of dye precursors in the formulation of commercial oxidation hair dyes, *Dyes Pigm.*, 41(1999), No. 1-2, p. 127.
[45] Y. Du, H.L. Chen, R.Z. Chen, and N.P. Xu, Synthesis of *p*-aminophenol from p-nitrophenol over nano-sized nickel catalysts, *Appl. Catal. A Gen.*, 277(2004), No. 1-2, p. 259.
[46] Z.Y. Zhang, C.L. Shao, P. Zou, P. Zhang, M.Y. Zhang, J.B. Mu, Z.C. Guo, X.H. Li, C.H. Wang, and Y.C. Liu, *In situ* assembly of well-dispersed gold nanoparticles on electrospun silica nanotubes for catalytic reduction of 4-nitrophenol, *Chem. Commun.*, 47(2011), No. 13, p. 3906.
[47] Y.W. Zhang, S. Liu, W.B. Lu, L. Wang, J.Q. Tian, and X.P. Sun, In situ green synthesis of Au nanostructures on graphene oxide and their application for catalytic reduction of 4-nitrophenol, *Catal. Sci. Technol.*, 1(2011), No. 7, art. No. 1142.
[48] J. Wang, X.B. Zhang, Z.L. Wang, L.M. Wang, W. Xing, and X. Liu, One-step and rapid synthesis of “clean” and monodisperse

dendritic Pt nanoparticles and their high performance toward methanol oxidation and p-nitrophenol reduction, *Nanoscale*, 4(2012), No. 5, p. 1549.

[49] G.T. Fu, L.F. Ding, Y. Chen, J. Lin, Y.W. Tang, and T.H. Lu, Facile water-based synthesis and catalytic properties of platinum–gold alloy nanocubes, *CrystEngComm*, 16(2014), No. 9, p. 1606.

[50] S.K. Ghosh, M. Mandal, S. Kundu, S. Nath, and T. Pal, Bimetallic Pt–Ni nanoparticles can catalyze reduction of aromatic nitro compounds by sodium borohydride in aqueous solution, *Appl. Catal. A Gen.*, 268(2004), No. 1-2, p. 61.

[51] M. Raula, D. Maity, M.H. Rashid, and T.K. Mandal, *In situ* formation of chiral core–shell nanostructures with raspberry-like gold cores and dense organic shells using catechin and their catalytic application, *J. Mater. Chem.*, 22(2012), No. 35, art. No. 18335.

[52] N. Sahiner, N. Karakoyun, D. Alpaslan, and N. Aktas, Biochar-embedded soft hydrogel and their use in ag nanoparticle preparation and reduction of 4-nitro phenol, *Int. J. Polym. Mater. Polym. Biomater*, 62(2013), No. 11, p. 590.

[53] M.H. Rashid, R.R. Bhattacharjee, A. Kotal, and T.K. Mandal, Synthesis of spongy gold nanocrystals with pronounced catalytic activities, *Langmuir*, 22(2006), No. 17, p. 7141.

[54] X. Guo, Q. Zhang, Y.H. Sun, Q. Zhao, and J. Yang, Lateral etching of core–shell Au@metal nanorods to metal-tipped Au nanorods with improved catalytic activity, *ACS Nano*, 6(2012), No. 2, p. 1165.